Structural Engineering and Mechanics, *Vol. 75, No. 1 (2020) 87-100*
DOI: https://doi.org/10.12989/sem.2020.75.1.087

Combination resonances of imperfect SSFG cylindrical shells rested on viscoelastic foundations

Kamran Foroutan[1a] and Habib Ahmadi*

Faculty of Mechanical and Mechatronics Engineering, Shahrood University of Technology, Shahrood, Iran

(Received September 5, 2019, Revised November 25, 2019, Accepted December 27, 2019)

Abstract. The present paper investigates the combination resonance behavior of imperfect spiral stiffened functionally graded (SSFG) cylindrical shells with internal and external functionally graded stiffeners under two-term large amplitude excitations. The structure is embedded within a generalized nonlinear viscoelastic foundation, which is composed of a two-parameter Winkler-Pasternak foundation augmented by a Kelvin-Voigt viscoelastic model with a nonlinear cubic stiffness, to account for the vibration hardening/softening phenomena and damping considerations. With regard to classical plate theory of shells, von-Kármán equation and Hook law, the relations of stress-strain are derived for shell and stiffeners. The spiral stiffeners of the cylindrical shell are modeled according to the smeared stiffener technique. According to the Galerkin method, the discretized motion equation is obtained. The combination resonance is obtained by using the multiple scales method. Finally, the influences of the stiffeners angles, foundation type, the nonlinear elastic foundation coefficients, material distribution, and excitation amplitude on the system resonances are investigated comprehensively.

Keywords: nonlinear vibrations; combination resonance behaviors; spiral stiffened FG cylindrical shell; multiple scales method; geometric imperfections; nonlinear viscoelastic foundation; two-term excitation

1. Introduction

Recently, the stiffened structures made of FG materials are extensively utilized in a wide range of engineering applications. Some researches have focused on the nonlinear resonant behavior of the homogeneous structures, the internal resonances for an axially moving cylinder were reported by Wang *et al.* (2013). Nonlinear vibration for fractionally damped and internal resonant of cylindrical shells under transverse excitations, respectively, was investigated by (Mahmoudkhani *et al.* 2011, Rodrigues *et al.* 2017). Ratnakar *et al*. (2007) addressed the dynamic combination resonance characteristics of doubly curved panels under the non-uniform tensile edge loading with damping. Huang *et al.* (2008) studied the parametric resonance of a rotating taper pre-twisted beam with cracks. The primary resonance behavior of axially moving beams with multiple concentrated masses was presented by Sarigul and Boyaci (2010).

In the field of laminated composite structures, the one-third subharmonic resonance behavior of laminated cylindrical shells under radial harmonic excitations was studied by Li *et al.* (2013). Gao *et al.* (2017) addressed the nonlinear vibration and stability analysis of the composite orthotropic plate rested on the elastic foundation in the thermal environment. The resonance behaviors of the laminated circular cylinder were investigated by (Zhang *et al.* 2018, Abe *et al.* 2007). Abe *et al.* (2007) derived the steady-state response by utilizing the shooting method. Kumar *et al.* (2015) reported the parametric resonance behavior of composite skew plate under non-uniform in-plane loading. The nonlinear free vibration of FG porous nanocomposite plates reinforced with a small amount of graphene platelets embedded in the elastic foundation was addressed by Gao *et al.* (2018a).

Some researchers have studied the vibration behavior analysis of the FG structures. For example, Gao and Yang (2019) presented the vibration analysis of the FG porous beams with interval material properties. The nonlinear dynamic buckling of FG porous beams was investigated by Gao *et al.* (2019). The investigation of resonant response for the FG shallow shells, employing the multiple scales procedure was addressed by Alijani *et al.* (2011). Sheng and Wang (2018a) reported the vibration of cylindrical shells with FG materials under the parametric and external loading. The nonlinear vibration of FG orthotropic cylinder with nonlinear/linear Winkler-type elastic foundations utilizing the first order shear deformation theory was studied by (Sofiyev 2016, Sofiyev *et al.* 2017). Gao *et al.* (2018b) investigated the nonlinear dynamic stability of the orthotropic FG cylindrical shell rested on the Winkler-Pasternak elastic foundation under linearly increasing load. The resonant analysis of the cylindrical shells with FG material under thermal environments was addressed by Du and Li (2013). Gao *et al.* (2018) reported the resonance responses of the FG porous cylindrical shell. In this study, the governing equations are derived using the Donnell's shell theory in conjunction with von Kármán's kinematic nonlinearity. Li *et al.* (2018) studied the parametric resonance analysis of cylindrical shells with FG material in thermal environments.

∗Corresponding author, Ph.D.
E-mail: habibahmadif@shahroodut.ac.ir
[a] Ph.D. Student

ISSN: 1225-4568 (Print), 1598-6217 (Online)

Review of the literature shows that few studies have been done on the resonant behavior of stiffened cylindrical shells with FG material. Some researches have been performed the resonant analysis of spiral stiffened cylindrical shells with FG material. The primary resonant behavior of stiffened FG cylindrical shells was addressed by Sheng and Wang (2018b), utilizing the multiple scales method. The resonant analysis of FG cylindrical shells with spiral stiffeners was addressed by (Ahmadi 2018, Ahmadi and Foroutan 2019a, b). Primary resonance for the system with the internal and external stiffeners was considered by (Ahmadi 2018, Ahmadi and Foroutan 2019a) with and without initial imperfection and nonlinear elastic foundation. Ahmadi and Foroutan (2019b) presented the Subharmonic and Superharmonic resonance of the system.

Recently, Ahmadi and Foroutan (2018c) investigated the combination resonance behavior of a cylindrical shell with porosity material under two-term excitation. Ahmadi and Foroutan (2018c) have assumed that the material to be porous and the spiral stiffener, initial imperfection, and nonlinear viscoelastic foundation have not been considered.

Previous works indicates that there is no study on the combination resonance analysis of the imperfect spiral stiffened cylindrical shells with FG material resting on nonlinear viscoelastic foundations with two-term large amplitude excitations. Therefore, the novelties of this work are as:

(1) Combination resonances formulation are analytically derived via the method of multiple scales for SSFG cylindrical shells,

(2) Incorporation of the effect of the surrounding nonlinear viscoelastic foundations on the SSFG cylindrical shells behavior,

(3) Both the stiffeners and shell are considered to be functionally graded,

(4) Investigation of the effect of the geometric imperfections, internal and external stiffeners on the SSFG cylindrical shells behavior.

For modeling of the system, the smeared stiffeners techniques and classical shell theory in conjunction with the relations of von Kármán's large deformation strain-displacement are used to obtain the nonlinear equations of the system. Then, Galerkin's method is used to discretize the domain. For investigation of the resonance behaviors of the system, the influences of angles of the spiral stiffeners, geometric imperfection, amplitudes of the two-term harmonic excitations, and volume fractions of the system are studied.

2. Description of the SSFG cylindrical shell with the nonlinear viscoelastic foundation

Fig. 1 illustrates the configuration of the spiral stiffened cylindrical shell with FG material resting on a nonlinear viscoelastic foundation which is a combination of Winkler-Pasternak and nonlinear Kelvin-Voight foundations. In other words, the considered viscoelastic foundation consists of Pasternak (k_s), Winkler (k_w), and nonlinear cubic (k_{nl}) stiffness and a viscous damping element. This type of foundation may cover many aspects of realistic foundations.

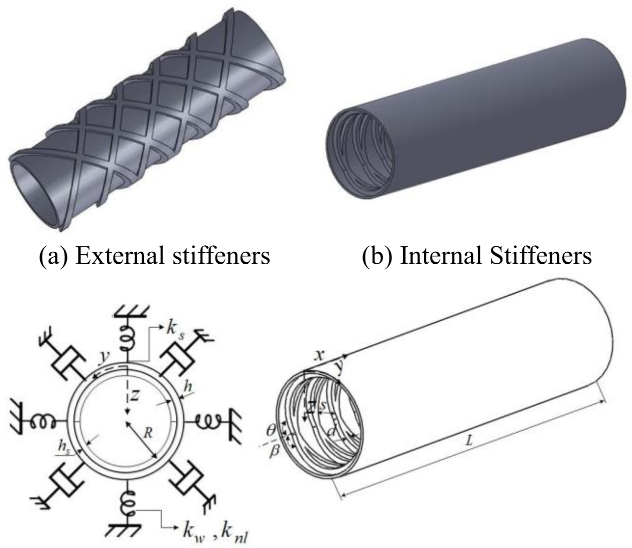

Fig. 1. Schematic of the FG cylindrical shell with the functionally graded spiral stiffeners and a nonlinear viscoelastic Kelvin-Voigt foundation

Considering Fig. 1, thickness, radius, and length of the cylindrical shell are denoted by *h, R,* and *L,* respectively. Also, the width, angles, thickness, and spacing of the stiffeners are indicated by *d*, (θ, β), h_s, and *s,* respectively. The stiffeners and cylindrical shell are constructed from a mixture of metal and ceramic.

The mass density and Young's modulus of the FG shell and stiffeners are defined as:

$$\begin{Bmatrix} E_{sh}(z) \\ \rho_{sh}(z) \end{Bmatrix} = \begin{Bmatrix} E_c \\ \rho_c \end{Bmatrix} + \begin{Bmatrix} E_{mc} \\ \rho_{mc} \end{Bmatrix} \left(\frac{2z+h}{2h} \right)^{K_{sh}} ; -\frac{h}{2} \le z \le \frac{h}{2} \quad \text{(1a)}$$

External stiffeners:

$$\begin{Bmatrix} E_{st}(z) \\ \rho_{st}(z) \end{Bmatrix} = \begin{Bmatrix} E_m \\ \rho_m \end{Bmatrix} + \begin{Bmatrix} E_{cm} \\ \rho_{cm} \end{Bmatrix} \left(\frac{2z+h}{2h_s} \right)^{K_{st}} ; -\left(\frac{h}{2} + h_s \right) \le z \le -\frac{h}{2} \quad \text{(1b)}$$

Internal stiffeners:

$$\begin{Bmatrix} E_{st}(z) \\ \rho_{st}(z) \end{Bmatrix} = \begin{Bmatrix} E_c \\ \rho_c \end{Bmatrix} + \begin{Bmatrix} E_{mc} \\ \rho_{mc} \end{Bmatrix} \left(\frac{2z+h}{2h_s} \right)^{K_{st}} ; \frac{h}{2} \le z \le \frac{h}{2} + h_s \quad \text{(1c)}$$

where e.g.,

$$E_{mc} = E_m - E_c \quad (2)$$

$K_{st} \ge 0$ and $K_{sh} \ge 0$ are the stiffeners and shell material power law index, respectively. $\rho_{sh}(z)$, $\rho_{st}(z)$ and $E_{sh}(z)$, $E_{st}(z)$ are mass densities and Young's modulus of the FG stiffeners and shell, respectively. The subscripts st, sh, *m* and *c* refer to the stiffeners, shell, metal and ceramic, respectively.

3. The theoretical formulation

In the light of von Kármán kinematic nonlinearity, the strain-displacement relation becomes (Wang *et al.* 2018, Zarouni *et al.* 2014)

$$\begin{Bmatrix}\varepsilon_x\\ \varepsilon_y\\ \gamma_{xy}\end{Bmatrix}=\begin{Bmatrix}\varepsilon_x^0\\ \varepsilon_y^0\\ \gamma_{xy}^0\end{Bmatrix}-z\begin{Bmatrix}\kappa_x\\ \kappa_y\\ 2\kappa_{xy}\end{Bmatrix} \tag{3}$$

$$\kappa_x=w_{,xx},\ \ \kappa_y=w_{,yy},\ \ \kappa_{xy}=w_{,xy}$$

where $\kappa_x,\kappa_y,\kappa_{xy}$ are the shell curvature changes and twist. γ_{xy}^0 is the shear strain, and ε_y^0, ε_x^0 are the normal strains. Moreover, the components of the strain on middle surface of shells are given by (Lezgy-Nazargah *et al.* 2011, Dat *et al.* 2019)

$$\begin{gathered}\varepsilon_x^0=u_{,x}+\frac{1}{2}w_{,x}^2+w_{,x}w_{,x}^*\\ \varepsilon_y^0=v_{,y}-\frac{w}{R}+\frac{1}{2}w_{,y}^2+w_{,y}w_{,y}^*\\ \gamma_{xy}^0=u_{,y}+v_{,x}+w_{,x}w_{,y}+w_{,y}w_{,x}^*+w_{,x}w_{,y}^*\end{gathered} \tag{4}$$

where $w=w(x,y)$, $u=u(x,y)$ and $v=v(x,y)$ are the displacement components along z, x and y axes, respectively, and $w^*=w^*(x,y)$ is the initial small geometric imperfection of the shell.

The compatibility equation according to Eq. (4) can be written as

$$\begin{aligned}\varepsilon_{x,yy}^0+\varepsilon_{y,xx}^0-\gamma_{xy,xy}^0=&-\tfrac{w_{,xx}}{R}+\left(w_{xy}+w_{xy}^*\right)^2\\ &-\left(w_{,xx}+w_{,xx}^*\right)\left(w_{,yy}+w_{yy}^*\right)\end{aligned} \tag{5}$$

The stress-strain relations with regard to the Hooke's law, for the cylindrical shell with FG material are

$$\begin{Bmatrix}\sigma_x^{sh}\\ \sigma_y^{sh}\\ \tau_{xy}^{sh}\end{Bmatrix}=\begin{bmatrix}\frac{E_{sh}(z)}{1-\nu^2} & \frac{\nu E_{sh}(z)}{1-\nu^2} & 0\\ \frac{\nu E_{sh}(z)}{1-\nu^2} & \frac{E_{sh}(z)}{1-\nu^2} & 0\\ 0 & 0 & \frac{E_{sh}(z)}{2(1+\nu)}\end{bmatrix}\begin{Bmatrix}\varepsilon_x\\ \varepsilon_y\\ \gamma_{xy}\end{Bmatrix} \tag{6}$$

On the other hand, the constitutive law of the spiral stiffeners is (Foroutan *et al.* 2018, Shaterzadeh and Foroutan 2016)

$$\begin{Bmatrix}\sigma_x^{st}\\ \sigma_y^{st}\\ \tau_{xy}^{st}\end{Bmatrix}=\begin{bmatrix}H_{11} & H_{12} & H_{13}\\ H_{21} & H_{22} & H_{23}\\ H_{31} & H_{32} & H_{33}\end{bmatrix}\begin{Bmatrix}h_1\varepsilon_x\\ h_2\varepsilon_y\\ h_3\gamma_{xy}\end{Bmatrix} \tag{7}$$

where ν is Poisson's ratio. $\sigma_x^{sh},\sigma_y^{sh}$ are the in-plane normal stresses and τ_{xy}^{sh} is the in-plane shearing stress of the cylindrical shell. H_{ij} $(i,j=1,2,3)$ and h_i $(i=1,2,3)$ are presented in appendix A. τ_{xy}^{st} is the in-plane shear stress and $\sigma_x^{st},\sigma_y^{st}$ are the in-plane normal stresses of the spiral stiffener. Utilizing the smeared stiffeners technique, the influence of the stiffeners on the cylindrical shell may be assumed. To obtain the resultant moments (M_x,M_y,M_{xy}) and forces (N_x,N_y,N_{xy}) for the spiral stiffened cylindrical shell with FG material, the equations of stress-strain (6) and (7) are integrated in thickness direction.

Neglecting the in-plane inertias, the equilibrium equations of cylindrical shells with regard to the classical shell theory are as (Bich *et al.* 2013, Van Dung and Hoa 2013, Dai *et al.* 2013)

$$\begin{gathered}N_{x,x}+N_{xy,y}=0\\ N_{xy,x}+N_{y,y}=0\\ M_{x,xx}+2M_{xy,xy}+M_{y,yy}+N_x\left(w_{,xx}+w_{,xx}^*\right)\\ +2N_{xy}\left(w_{,xy}+w_{,xy}^*\right)+N_y\left(w_{,yy}+w_{,yy}^*+1/R\right)\\ -k_w w+k_s\left(w_{,xx}+w_{,yy}\right)+k_{nl}w^3+F(t)\\ =\rho_1 w_{,tt}+2\rho_1\hat{c}w_{,t}\end{gathered} \tag{8}$$

where $\hat{c}$ is the coefficient of the viscous damping. The harmonic excitation $F(t)$ and the mass density ρ_1 are as follows

External stiffeners:

$$\rho_1=\left(\rho_c+\frac{\rho_{mc}}{K_{sh}+1}\right)h+2\left(\rho_m(T)+\frac{\rho_{cm}}{K_{st}+1}\right)\frac{dh_s}{S} \tag{9a}$$

Internal stiffeners:

$$\rho_1=\left(\rho_m+\frac{\rho_{cm}}{K_{sh}+1}\right)h+2\left(\rho_c+\frac{\rho_{mc}}{K_{st}+1}\right)\frac{dh_s}{S} \tag{9b}$$

Harmonic excitation:

$$F(t)=-Q_1\cos(\Omega_1 t+\theta_1)-Q_2\cos(\Omega_2 t+\theta_2) \tag{9c}$$

where Q_1 and Q_2 are the load amplitudes, the first two equations of Eq. (8) may be satisfied merely by definition of the following stress function (ψ)

$$N_x=\psi_{,yy};\ \ N_y=\psi_{,xx};\ \ N_{xy}=-\psi_{,xy} \tag{10}$$

To find the compatibility equation with regard to the lateral deflection w and the stress function ψ, first, the strain components must be obtained in terms of the resultant forces. So, according to Eq. (10), the strain components may be expressed in terms of the stress function. Substituting these relations into the compatibility Eq. (5), omits partial differentials of the in-plane displacement components; so that, the compatibility equation may be represented in terms of w and ψ (Foroutan *et al.* 2018, Shaterzadeh and Foroutan 2016)

$$\begin{gathered}J_{11}^*\psi_{,xxxx}+(J_{33}^*-J_{12}^*+J_{21}^*)\psi_{,xxyy}+J_{22}^*\psi_{,yyyy}\\ +J_{21}^{**}w_{,xxxx}+(J_{11}^{**}+J_{22}^{**}-2J_{36}^{**})w_{,xxyy}\\ +J_{12}^{**}w_{,yyyy}+\frac{1}{R}w_{,xx}+\left[w_{,xy}^2-w_{,xx}w_{,yy}\right]\\ -2w_{,xy}w_{,xy}^*+w_{,xx}w_{,xx}^*+w_{,yy}w_{,yy}^*=0\end{gathered} \tag{11}$$

where J_{ij}^*,J_{ij}^{**} are presented in the Appendix B.

Similar to the above discussion, by substituting the moment resultants into the third part of Eq. (8) and utilizing Eqs. (4) and (9), yields (Foroutan *et al.* 2018, Pendhari *et al.* 2012)

$$\begin{gathered}\rho_1 w_{,tt}+2\rho_1\hat{c}w_{,t}+A_{11}^{**}w_{,xxxx}\\ +(A_{12}^{**}+A_{21}^{**}+4A_{36}^{**})w_{,xxyy}+A_{22}^{**}w_{,yyyy}\\ -A_{21}^*\psi_{,xxxx}-(A_{11}^*+A_{22}^*-2A_{36}^*)\psi_{,xxyy}\end{gathered} \tag{12}$$

$$-A_{12}^{*}\psi_{,yyyy}-\frac{1}{R}\psi_{,xx}-\psi_{,yy}\left(w_{,xx}+w_{,xx}^{*}\right)$$
$$+2\psi_{,xy}\left(w_{,xy}+w_{,xy}^{*}\right)-\psi_{,xx}\left(w_{,yy}+w_{,yy}^{*}\right)$$
$$-Q_1\cos(\Omega_1 t+\theta_1)-Q_2\cos(\Omega_2 t+\theta_2)$$
$$+k_w w-k_s\left(w_{,xx}+w_{,yy}\right)-k_{nl}w^3=0$$

where the coefficients A_{ij}^{*} and A_{ij}^{**} are presented in the Appendix B.

4. The semi-analytical solutions of the problem

The forms of the initial imperfection and the approximate solution of the simply supported SSFG cylindrical shells are considered as follows (Dai *et al.* 2013, Wang et al. 2019, Pendhari *et al.* 2012) to solve Eq. (12)

$$\begin{Bmatrix} w(x,y,t) \\ w^{*}(x,y) \end{Bmatrix}=\begin{Bmatrix} W_{mn}(t) \\ \mu h \end{Bmatrix}\sin\frac{m\pi x}{L}\sin\frac{ny}{R} \tag{13}$$

where n and m are numbers of the half and full deformation waves in the circumferential and axial directions, respectively. n is the imperfection parameter. $W_{mn}(t)$ represents the deflection amplitude. In writing Eq. (13) the concept of amplitude magnification is employed wherein, shape modes of the geometric imperfections that are identical to the resonance mode are magnified (Eslami *et al.* 1998, Shariyat *et al.* 2011). In other words, although the vibration may take place in a multi-mode condition, in the resonance/buckling conditions, there is a distinctly dominant instability mode. For this reason, almost all the performed instability (buckling or resonance) studies by prominent researchers have been accomplished based on this idea (Shen 2017, Eslami 2018).

Substituting Eq. (13) in Eq. (11), and then solving the resultant equation for ψ, yields

$$\psi=\quad \psi_1\cos\frac{2m\pi x}{L}+\psi_2\cos\frac{2ny}{R} -\psi_3\sin\frac{m\pi x}{L}\sin\frac{ny}{R} \tag{14}$$

The $\psi_i(i=1,2,3)$ are as follows

$$\psi_1=\frac{n^2\lambda^2}{32J_{11}^{*}m^2\pi^2}W_{mn}(t)(W_{mn}(t)+\mu h)(W_{mn}(t)+2\mu h)$$
$$\psi_2=\frac{m^2\pi^2}{32J_{22}^{*}n^2\lambda^2}W_{mn}(t)(W_{mn}(t)+\mu h)(W_{mn}(t)+2\mu h) \tag{15}$$
$$\psi_2=\frac{B}{A}W_{mn}(t)$$

If Eq. (12) is denoted by $\Gamma=0$, the relevant W_{mn} terms may be found, based on Galerkin's method

$$\int_0^L\int_0^{2\pi R}\sin\frac{m\pi x}{L}\sin\frac{ny}{R}\Gamma dydx \tag{16}$$

After substitution of Eqs. (13) and (14) into Eq. (12), the following results may be obtained, after carrying out Galerkin's orthogonality integration appeared in Eq. (16)

$$\ddot{W}_{mn}+2\hat{c}\dot{W}_{mn}+\omega_{mn}^2W_{mn}+\hat{a}_2W_{mn}^2+\hat{a}_3W_{mn}^3= k_1\cos(\Omega_1 t+\theta_1)+k_2\cos(\Omega_2 t+\theta_2) \tag{17}$$

where

$$\omega_{mn}=\left[\frac{1}{L^4\rho_1}\left(D+\frac{BB^{*}}{A}+2G\mu^2h^2+L^4k_w +L^2k_s[(\lambda n)^2+(m\pi)^2]\right)\right]^{\frac{1}{2}} \tag{18}$$
$$k_1=\frac{Q_1}{L^4\rho_1},\quad k_2=\frac{Q_2}{L^4\rho_1}$$

where B, A, D and B^{*} are presented in Appendix B. ω_{mn} is the dominant natural frequency of the cylindrical shell, and $\hat{a}_2$ and $\hat{a}_3$ expressions that are case-dependent and defined in the sequel.

5. The semi-analytical solutions of the problem

According to Eq. (17), the discretized motion equation of system consists of quadratic and cubic nonlinearities. Therefore the resonances analysis can be performed based on quadratic and cubic nonlinearities. To this end, the considered nonlinearity and the damping terms must be assumed in the same order. Accordingly, to analyze the combination resonances generated by the cubic nonlinearity, the damping and cubic nonlinearity (W_{mn}^3) terms of Eq. (17) must be set in the same order (Nayfeh and Mook, 1995). In this case, the proper $\hat{a}_2$ and $\hat{a}_3$ parameters become

$$\hat{c}=\epsilon c,\quad \hat{a}_2=\epsilon^2\alpha_2,\quad \hat{a}_3=\epsilon\alpha_3 \tag{19}$$

where

$$\alpha_2=\frac{2G\mu h}{L^4\rho_1},\alpha_3=\frac{G}{L^4\rho_1}+\frac{9}{16\rho_1}k_{nl} \tag{20}$$

Also, dimensionless parameter $\epsilon\ll 1$ is the order of the motion amplitude, and G is defined in Appendix B.

Substituting Eq. (19) in Eq. (17), the nonlinear equation of the system becomes as follows

$$\ddot{W}_{mn}+2\epsilon c\dot{W}_{mn}+\omega_{mn}^2W_{mn}+\epsilon^2\alpha_2W_{mn}^2 +\epsilon\alpha_3W_{mn}^3=k_1\cos(\Omega_1 t+\theta_1)+k_2\cos(\Omega_2 t+\theta_2) \tag{21}$$

5.1 Solution of the resulting nonlinear equation by the multiple scales method

For solving Eq. (21) utilizing the multiple scales method, an expansion in the following form is adopted

$$\mathrm{W}(t,\epsilon)=W_0(T_0,T_1)+\epsilon W_1(T_0,T_1)+\cdots \tag{22}$$

where the new time-dependent variables T_0 and T_1 are introduced as

$$T_n=\epsilon^n t;\qquad n=0,1 \tag{23}$$

Substitution of Eq. (22) in Eq. (21), and then equating the coefficients of the ϵ^0 and ϵ (perturbation coefficients) to zero leads to:

$$D_0^2 W_0 + \omega_{mn}^2 W_0 = k_1 \cos(\Omega_1 t + \theta_1) + k_2 \cos(\Omega_2 t + \theta_2) \tag{24}$$

$$D_0^2 W_1 + \omega_{mn}^2 W_1 = -2D_0 D_1 W_0 - 2cD_0 W_0 - \alpha_3 W_0^3 \tag{25}$$

where

$$D_n = \frac{\partial}{\partial T_n}; \qquad n = 0,1 \tag{26}$$

The general solution of Eq. (24) is

$$W_0 = A(T_1) e^{i\omega_{mn} T_0} + \Lambda_1 e^{i\Omega_1 T_0} + \Lambda_2 e^{i\Omega_2 T_0} + \text{c.c.} \tag{27}$$

In Eq. (27), c.c. is the complex conjugate and

$$\Lambda_1 = \frac{k_1 e^{i\theta_1}}{2(\omega_{mn}^2 - \Omega_1^2)}, \quad \Lambda_2 = \frac{k_2 e^{i\theta_2}}{2(\omega_{mn}^2 - \Omega_2^2)} \tag{28}$$

Substituting Eq. (27) in Eq. (25), yields

$$\begin{aligned} D_0^2 W_1 + \omega_{mn}^2 W_1 = & -[2i\omega_{mn}(A' + cA) \\ & + 3\alpha_3(A\Lambda + 2\Lambda_1\overline{\Lambda}_1 + 2\Lambda_2\overline{\Lambda}_2)A] e^{i\omega_{mn}T_0} \\ & -\Lambda_1[2i\Omega_1 c + 3\alpha_3(2A\bar{A} + \Lambda_1\overline{\Lambda}_1 + 2\Lambda_2\overline{\Lambda}_2)] e^{i\Omega_1 T_0} \\ & -\Lambda_2[2i\Omega_1 c + 3\alpha_3(2A\bar{A} + 2\Lambda_1\overline{\Lambda}_1 + \Lambda_2\overline{\Lambda}_2)] e^{i\Omega_2 T_0} \\ & -\alpha_3\{A^3 e^{3i\omega_{mn}T_0} + \Lambda_1^3 e^{3i\Omega_1 T_0} + \Lambda_2^3 e^{3i\Omega_2 T_0} \\ & + 3A^2\Lambda_1 e^{i(2\omega_{mn}+\Omega_1)T_0} + 3A^2\Lambda_2 e^{i(2\omega_{mn}+\Omega_2)T_0} \\ & + 3A^2\overline{\Lambda}_1 e^{i(2\omega_{mn}-\Omega_1)T_0} + 3A^2\overline{\Lambda}_2 e^{i(2\omega_{mn}-\Omega_2)T_0} \\ & + 3A\Lambda_1^2 e^{i(\omega_{mn}+2\Omega_1)T_0} + 3A\Lambda_2^2 e^{i(\omega_{mn}+2\Omega_2)T_0} \\ & + 3A\overline{\Lambda}_1^2 e^{i(\omega_{mn}-2\Omega_1)T_0} + 6A\overline{\Lambda}_1\Lambda_2 e^{i(\omega_{mn}-\Omega_1+\Omega_2)T_0} \\ & + 6A\Lambda_1\overline{\Lambda}_2 e^{i(\omega_{mn}+\Omega_1-\Omega_2)T_0} + 3\Lambda_1^2\Lambda_2 e^{i(2\Omega_1+\Omega_2)T_0} \\ & + 3\Lambda_1^2\overline{\Lambda}_2 e^{i(2\Omega_1-\Omega_2)T_0} + 3\Lambda_1\Lambda_2^2 e^{i(\Omega_1+2\Omega_2)T_0} \\ & + 3\overline{\Lambda}_1\Lambda_2^2 e^{i(2\Omega_2-\Omega_1)T_0}\} + \text{c.c.} \end{aligned} \tag{29}$$

Eq. (29) shows the several resonant combinations that some of them are monofrequency excitations and others are multifrequency excitations. These combinations can be considered in the following form

Subharmonic resonance:

$$\omega_{mn} \approx \frac{1}{3}\Omega_k \tag{30}$$

Superharmonic resonance:

$$\omega_{mn} \approx 3\Omega_k \tag{31}$$

Combination resonance:

$$\begin{gathered} \omega_{mn} \approx |\pm 2\Omega_l \pm \Omega_k| \\ \omega_{mn} \approx \frac{1}{2}(\Omega_l \pm \Omega_k) \end{gathered} \tag{32}$$

where $k, l = 1,2$. It should be noted that for a multifrequency excitation, several resonant conditions may be occurred simultaneously; i.e. both superharmonic and combination resonances or both subharmonic and superharmonic resonances, etc. can occur simultaneously. For a two-term excitation, maximum two resonances can be occurred simultaneously. If excitation frequencies are depicted by Ω_1 and Ω_2 where $\Omega_2 > \Omega_1$, the possible secondary resonances can be occurred in the following form

$$\begin{gathered} \omega_{mn} \approx 3\Omega_1 \text{ or } 3\Omega_2 \\ \omega_{mn} \approx \frac{1}{3}\Omega_1 \text{ or } \frac{1}{3}\Omega_2 \\ \omega_{mn} \approx \Omega_2 \pm 2\Omega_1 \text{ or } 2\Omega_1 - \Omega_2 \\ \omega_{mn} \approx 2\Omega_2 \pm \Omega_1 \\ \omega_{mn} \approx \frac{1}{2}(\Omega_2 \pm \Omega_1) \end{gathered} \tag{33}$$

Investigation of these resonances shows that more than one of them occur simultaneously if

$$\begin{aligned} &\text{(a)}\ \ \Omega_2 \approx 9\Omega_1 \approx 3\omega_{mn} \\ &\text{(b)}\ \ \Omega_2 \approx \Omega_1 \approx 3\omega_{mn} \\ &\text{(c)}\ \ \Omega_2 \approx \Omega_1 \approx \tfrac{1}{3}\omega_{mn} \\ &\text{(d)}\ \ \Omega_2 \approx 5\Omega_1 \approx \tfrac{5}{3}\omega_{mn} \\ &\text{(e)}\ \ \Omega_2 \approx 7\Omega_1 \approx \tfrac{7}{3}\omega_{mn} \\ &\text{(f)}\ \ \Omega_2 \approx 2\Omega_1 \approx \tfrac{2}{3}\omega_{mn} \\ &\text{(g)}\ \ \Omega_2 \approx \tfrac{7}{3}\Omega_1 \approx 7\omega_{mn} \\ &\text{(h)}\ \ \Omega_2 \approx \tfrac{5}{3}\Omega_1 \approx 5\omega_{mn} \end{aligned} \tag{34}$$

Here, the case $\omega_{mn} \approx \Omega_2 + 2\Omega_1$ is selected. For frequency analysis purposes, the frequency of the excitation may be detuned by means a of a σ parameter, which defines the nearness of $\Omega_2 + 2\Omega_1$ to ω_{mn} as follows

$$\omega_{mn} = \Omega_2 + 2\Omega_1 - \epsilon\sigma \tag{35}$$

Now, Eq. (35) is substituted into Eq. (29), and then the coefficient of secular terms (i.e., $\exp(i\omega_{mn}T_0)$) is set equal to zero as

$$2i\omega_{mn}(A' + cA) + 3\alpha_3(A\Lambda + 2\Lambda_1\overline{\Lambda}_1 + 2\Lambda_2\overline{\Lambda}_2)A + 3\alpha_3\Lambda_1^2\Lambda_2 e^{i\sigma T_1} = 0 \tag{36}$$

To find the response of Eq. (36), A is assumed in the following polar form

$$A = \frac{1}{2} a e^{i\beta} \tag{37}$$

where $\beta(T_1)$ and $a(T_1)$ are real quantities.

After substitution Eq. (37) into Eq. (36), the imaginary and real parts of the resulted equation are obtained as

$$a' = -\mu a - \alpha_3\, \Gamma_1 \sin(\gamma) \tag{38}$$

$$a\gamma' = (\sigma - \alpha_3\, \Gamma_2) a - \frac{3\alpha_3}{8\omega_{mn}} a^3 - \alpha_3\, \Gamma_1 \cos(\gamma) \tag{39}$$

Table 1 Comparison of the natural frequencies of cylindrical shell $L = 0.2$ m, $R = 0.1$ m, $h = 0.247 \times 10^{-3}$ m, $m = 1$, $E = 7.12 \times 10^{10}$ N/m^2, $\rho = 2796$ kg/m^3, $\nu = 0.31$)

m	n	Present	Pellicano (2007)	Errors (%)	Qin *et al.* (2017)	Errors (%)
1	7	486.0	484.6	0.2	484.6	0.2
1	8	490.3	489.6	0.1	489.6	0.1
1	9	545.8	546.2	0.07	546.2	0.07
1	6	555.8	553.3	0.4	553.3	0.4
1	10	634.8	636.8	0.3	636.8	0.3
2	10	962.3	968.1	0.5	968.1	0.5
2	11	976.6	983.4	0.6	983.4	0.6

where

$$\Gamma_1 = \frac{3}{8} k_1^2 k_2 \omega_{mn}^{-1} (\omega_{mn}^2 - \Omega_1^2)^{-2} (\omega_{mn}^2 - \Omega_2^2)^{-1}$$

$$\Gamma_2 = \frac{3}{4} \omega_{mn}^{-1} [k_1^2 (\omega_{mn}^2 - \Omega_1^2)^{-2} + k_2^2 (\omega_{mn}^2 - \Omega_2^2)^{-2}] \tag{40}$$

$$\gamma = \sigma T_1 - \beta + 2\theta_1 + \theta_2$$

When $a', \gamma' = 0$, the steady-state motion happens. In this case, singularities occur in Eqs. (38) and (39). The frequency response may be computed by summing the squares of the resultant equations in the steady-state condition as

$$\left[c^2 + \left(\sigma - \alpha_3 \Gamma_2 - \frac{3\alpha_3}{8\omega_{mn}} a^2 \right)^2 \right] a^2 = \alpha_3^2 \Gamma_1^2 \tag{41}$$

6. Results and discussions

6.1 Verification of the results

Results are first verified by those published already by other researchers, for special cases. First, the obtained natural frequencies of isotropic cylindrical shells are validated with those presented by (Pellicano 2007, Qin *et al.* 2017). Furthermore, the present results of the natural frequencies are compared in Table 2, for the nonlinear vibration behavior of a cylindrical shell with FG material which is stiffened by stringer and ring, with those accomplished already by Van Dung and Nam (2014).

For more validation of the approach, the present results of the dimensionless natural frequencies ($\bar{\omega}_{mn} = \omega_{mn} R \sqrt{(1-\nu^2)\frac{\rho}{E}}$) are compared in Table 3 with those of the nonlinear vibration behavior of a homogeneous cylindrical shell rested on a Winkler foundation accomplished already by (Sofiyev *et al.* 2009, Van Dung and Nam 2014). Also, results of a stiffened cylindrical shell are compared with the experimentally validated results of Mustafa and Ali (1989) in Table 4. It may easily be noted that there is a good agreement among these results.

Table 2 Comparison of the natural frequencies of stiffened FG cylindrical shell ($L = 0.75$ m, $R = 0.5$ m, $R/h = 250$, $m = 1$, $E_m = 7 \times 10^{10}$ N/m^2, $\rho_m = 2702$ kg/m^3, $E_c = 38 \times 10^{10}$ N/m^2, $\rho_c = 3800$ kg/m^3, $\nu = 0.3$, $d_s = d_r = 0.0025$ m, $h_s = h_r = 0.01$ m)

	Present	Van Dung and Nam (2014)	Errors (%)
Un-stiffened			
	1654.05	1654.05	0.00
Internal stiffeners			
	2539.43	2539.43	0.00
External stiffeners			
	2518.90	2518.90	0.00

Table 3 A comparison of the dimensionless natural frequencies of the cylindrical shell resting on the Winkler foundation ($L/R = 2$, $R/h = 100$, $k_w = 10^4$ N/m^3)

(m,n)	Present	Sofiyev *et al.* (2009)	Errors (%)	Van Dung and Nam (2014)	Errors (%)
(1,1)	0.67480	0.67921	0.65	0.67480	0.00
(1,2)	0.36223	0.36463	0.66	0.36223	0.00
(1,3)	0.20670	0.20804	0.65	0.20670	0.00

Table 4 Results of the natural frequencies of the stiffened cylindrical shell ($L = 0.6096$ m , $R = 0.242$ m , $h = 0.65 \times 10^{-3}$ m, $E = 68.95 \times 10^9$ N/m^2, $\rho = 2714$ kg/m^3, $\nu = 0.3$, $n_s = 60$)

(m,n)	Present	Mustafa and Ali (1989)	Errors (%)
(1,5)	228.1	226	0.9
(1,6)	189.4	191	0.8
(1,7)	174.0	179	2.4

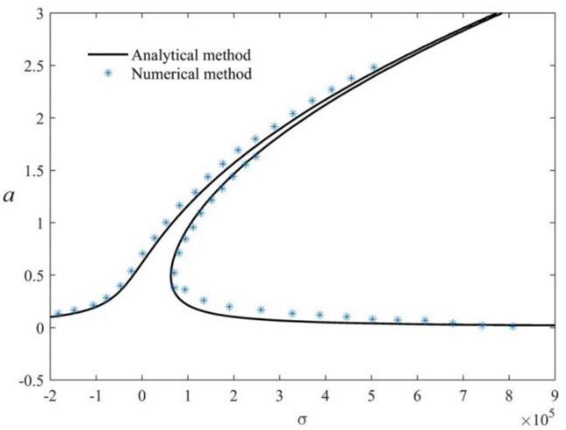

Fig. 2 A comparison between the analytical and numerical frequency response curves ($\theta = 0°, \beta = 90°, K_{sh} = K_{st} = 1$). The amplitude is in meters.

Finally, a numerical method is used to verify the results of the proposed analytical method for the combination

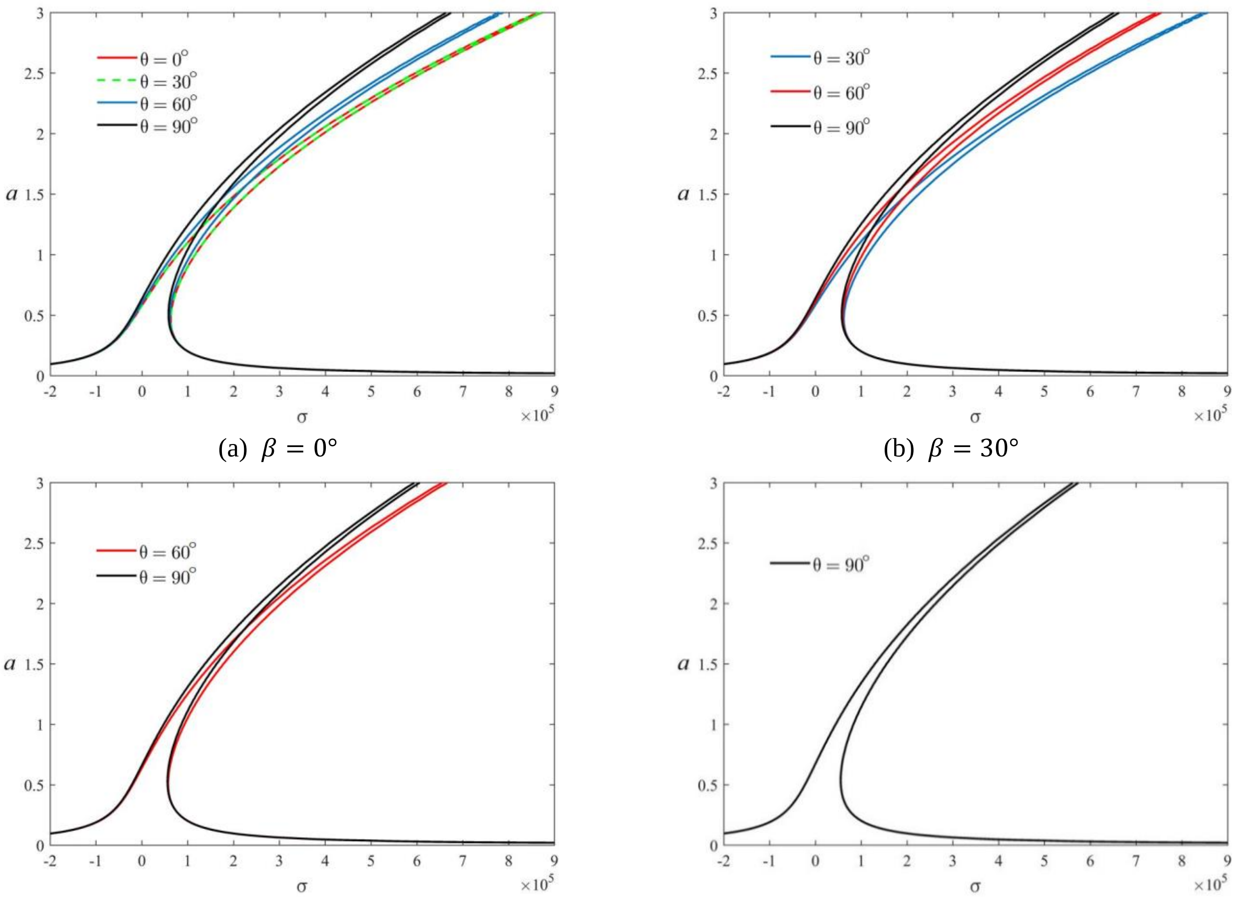

(a) $\beta = 0°$ (b) $\beta = 30°$

(c) $\beta = 60°$ (d) $\beta = 90°$

Fig. 3 Frequency response curves of the external SSFG cylindrical shell ($K_{sh} = K_{st} = 1$)

resonance. Hereafter, the geometric parameters and material parameters listed in Table 5 will be used for the simulation results.

In the numerical procedure, Eq. (17) has been solved via the fourth-order Runge-Kutta procedure. In this method, the maximum amplitude has been detected for various magnitudes of the excitation, based on the time responses, using the $W(0) = 0$ and $\dot{W}(0) = 0$ initial conditions. The analytical and numerical frequency response curves are compared in Fig. 2. This figure shows that the results of the analytical method are almost similar to the results of the numerical method, especially, in the vicinity of the instability.

6.2 Comprehensive parametric studies on the combination resonances

Now, the effects of various factors on the spirally stiffened imperfect FG cylindrical shells surrounded by nonlinear viscoelastic foundations under two-term large amplitude excitations are illustrated. In this regard, the influences of the material and geometric parameters, initial imperfection, and nonlinear viscoelastic foundation are considered.

The influence of the stiffener angles on the response of the amplitude-frequency for the external and internal spiral stiffened cylindrical shell with FG material is displayed in Figs. 3 and 4, respectively. Regarding these figures, the hardening nonlinearity behavior of the system is more than other cases when angles of the stiffener, i.e., θ and β (Fig. 1) are between 0° and 30° whereas, the hardening nonlinearity behavior is less than other cases when the stiffener angles are between 60° and 90°.

Fig. 5 illustrates the effect of the volume fraction index ($K_{sh} = K_{st}$) on the frequency-amplitude for combination resonances of the imperfect spiral stiffened cylindrical shell with FG material. According to Fig. 5a, the nonlinearity behavior of the system with external stiffeners is increased when the volume fraction index is increased. Whereas, according to Fig. 5b, the nonlinearity behavior of the system with internal stiffeners is decreased when the volume fraction index is increased.

Fig. 6 illustrates the influence of the material distribution of the internal stiffeners and shell on the amplitude-frequency of system. As can be seen, the ceramic cylindrical shells with the metal stiffeners have more hardening nonlinearity behavior than others, and the metallic cylindrical shells with the ceramic stiffeners have less hardening nonlinearity behavior than others.

Fig. 7 illustrates the effects of the imperfection amplitude parameter (μ) on the behavior of frequency-amplitude of the spiral stiffened cylindrical shell with FG material. The hardening nonlinearity behavior of SSFG system increases by increasing this parameter.

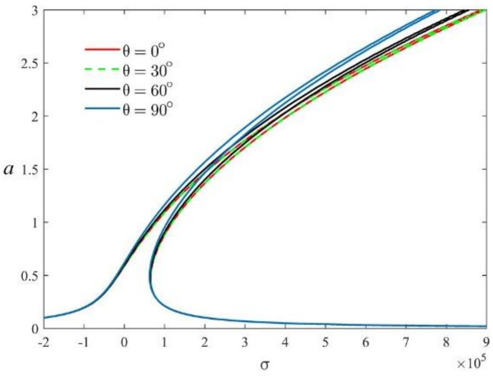

(a) $\beta = 0°$

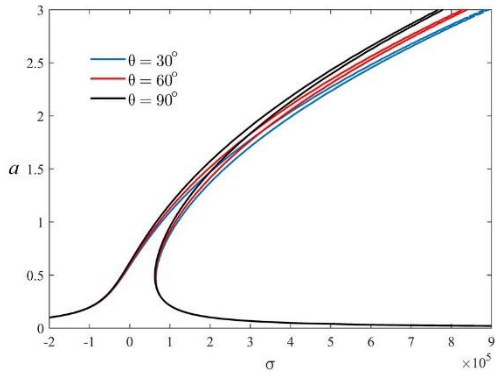

(b) $\beta = 30°$

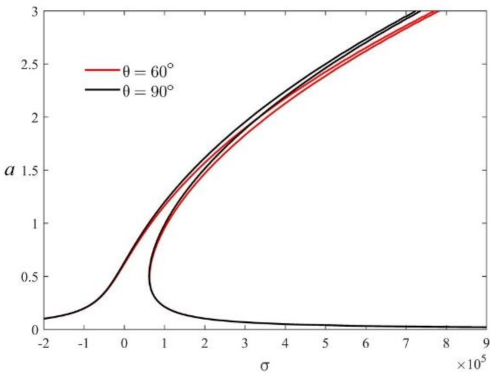

(c) $\beta = 60°$

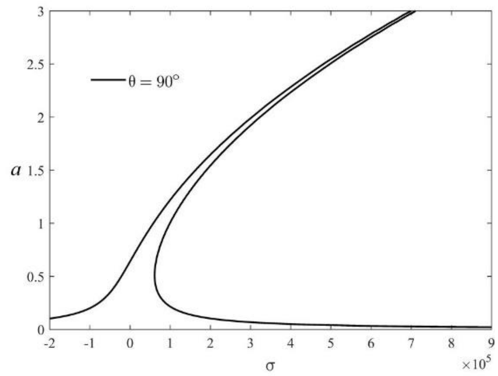

(d) $\beta = 90°$

Fig. 4 Frequency response curves of the internal SSFG cylindrical shell ($K_{sh} = K_{st} = 1$)

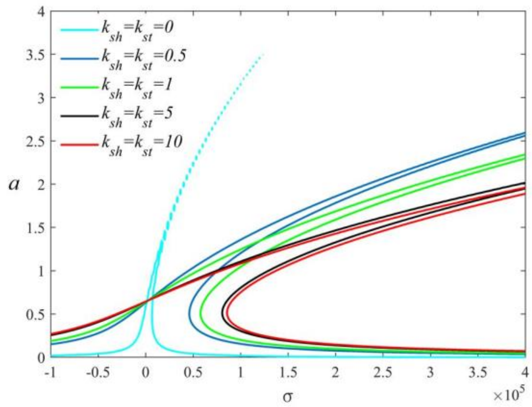

(a) External stiffeners

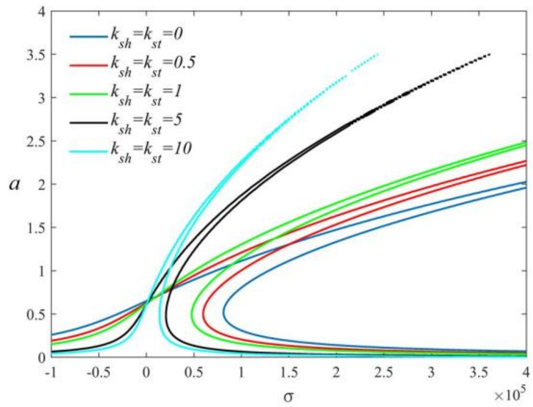

(b) Internal stiffeners

Fig. 5 Effect of the volume fraction on the frequency response curves of the SSFG cylindrical shell ($K_{sh} = K_{st} = 1, \theta = 0°, \beta = 90°$)

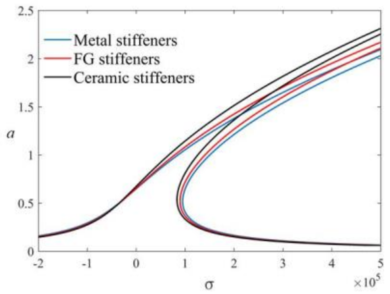

(a) Ceramic shell

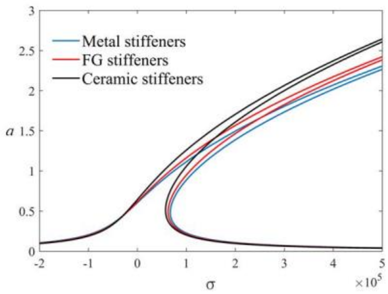

(b) FG shell

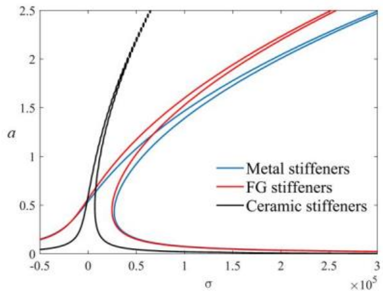

(c) Metal shell

Fig. 6 Effect of material properties on the frequency response curves of the internal SSFG cylindrical shells ($\theta = 0°, \beta = 90°$)

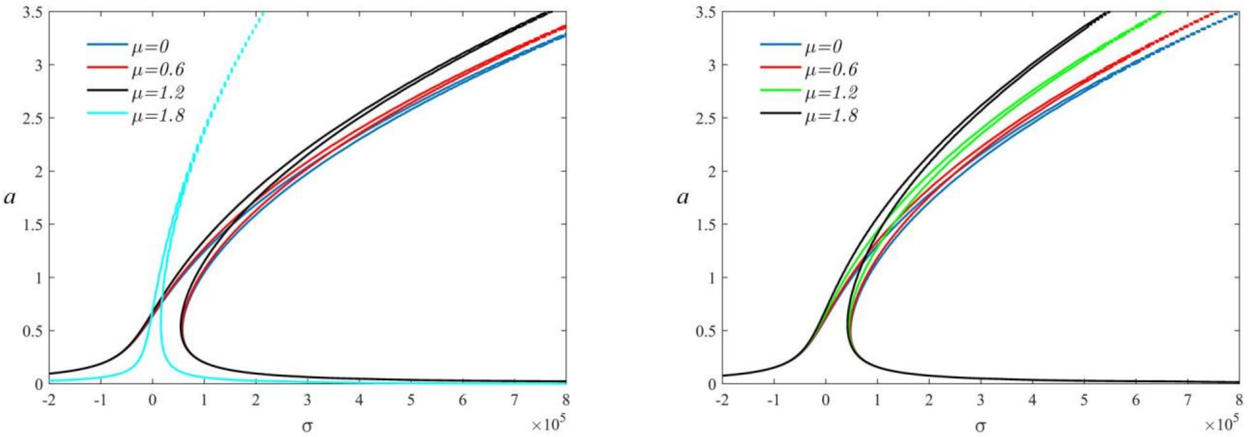

(a) External stiffeners (b) Internal stiffeners

Fig. 7 Effect of the imperfection amplitude on the frequency response curves of the SSFG cylindrical shell ($K = K_s = 1, \theta = 0°, \beta = 90°$)

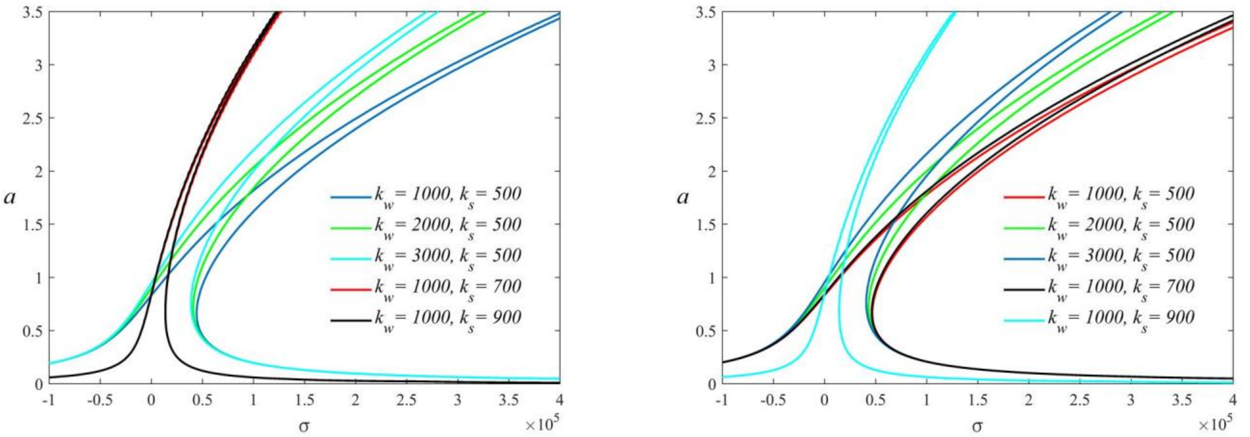

(a) External stiffeners (b) Internal stiffeners

Fig. 8 Effect of the coefficient of the linear elastic foundation on the frequency response curves of the SSFG cylindrical shell ($K = K_s = 1, \theta = 0°, \beta = 90°$)

Fig. 8 shows the influence of the coefficient of the linear elastic foundation on the variations of the amplitude-frequency for the spiral stiffened cylindrical shell with FG material. This figure shows the hardening nonlinearity behavior of the system with the Pasternak foundation is larger than the hardening nonlinearity behavior of the system with the Winkler's foundation.

Fig. 9 displays the influence of nonlinear and linear stiffness of the foundation on the amplitude-frequency response. According to this figure, the negative and positive nonlinear stiffness is decreased and increased the hardening nonlinearity behavior of the system, respectively. Furthermore, the negative nonlinear elastic foundation increases the peak value. Also, regarding this figure, the hardening nonlinearity behavior of system with the linear elastic foundation is decreased more than the system with nonlinear elastic foundation.

The influence of the excitation amplitudes Γ_1 and Γ_2 on the frequency-response for combination resonances of the spiral stiffened cylindrical shell with FG material is illustrated in Figs. 10 and 11, respectively. As shown in Fig. 10, by increasing Γ_1, the curve of frequency-response is scaled up. Whereas Fig. 11 shows that by increasing Γ_2, the jumping phenomenon is transferred to higher values of σ.

7. Conclusions

A semi-analytical approach is developed to investigate the combination resonance of imperfect spiral stiffened cylindrical shell with FG material resting on Winkler-Pasternak-Kelvin-Voigt viscoelastic foundations with cubic nonlinear stiffness, under two-term harmonic excitations. Material distribution of both the stiffeners and the shell were graded in the thickness direction. von Kármán-type of kinematic nonlinearity was adopted to enable large deformations analyses. Then, the coupled nonlinear response of the problem was obtained using the concept of stress function, Galerkin's orthogonality, and the smeared stiffeners technique. To determine the system response for the combination resonances, the multiple scales method was utilized. Then, the influences of various material, geometric, loading, and foundation parameters were investigated. Some of the main conclusions may be summarized in the following form:

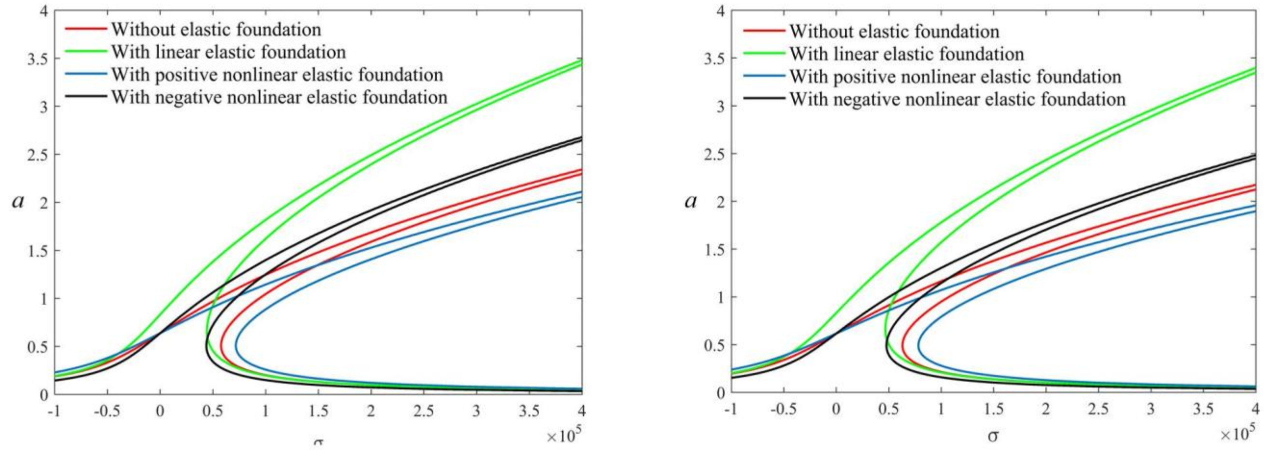

(a) External stiffeners (b) Internal stiffeners

Fig. 9 Effect of the nonlinear and linear stiffness of the foundation on the frequency response curves of the SSFG cylindrical shell ($K = K_s = 1, \theta = 0°, \beta = 90°$)

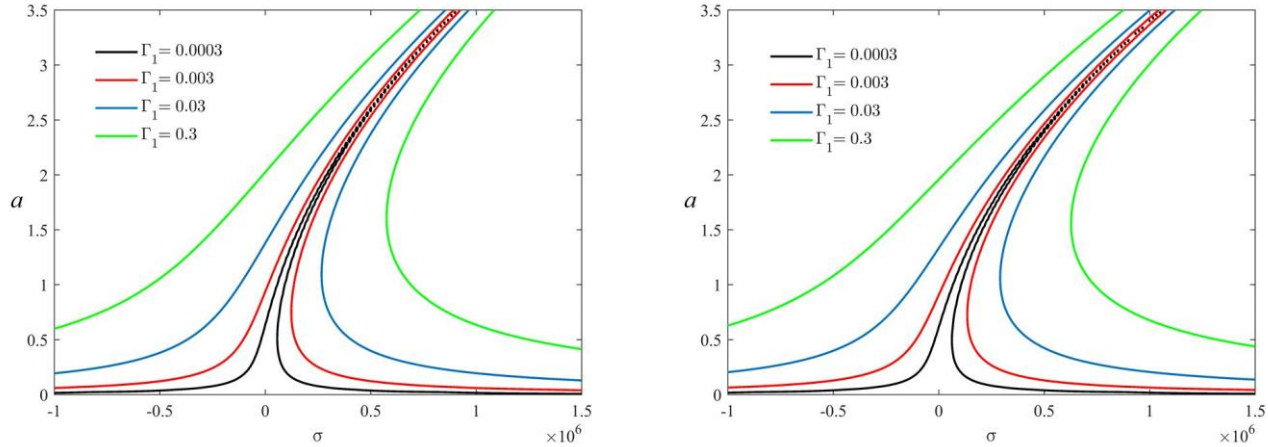

(a) External stiffeners (b) Internal stiffeners

Fig. 10 Effect of the excitation amplitudes on the frequency response of the SSFG cylindrical shell ($K = K_s = 1, \theta = 0°, \beta = 90°$)

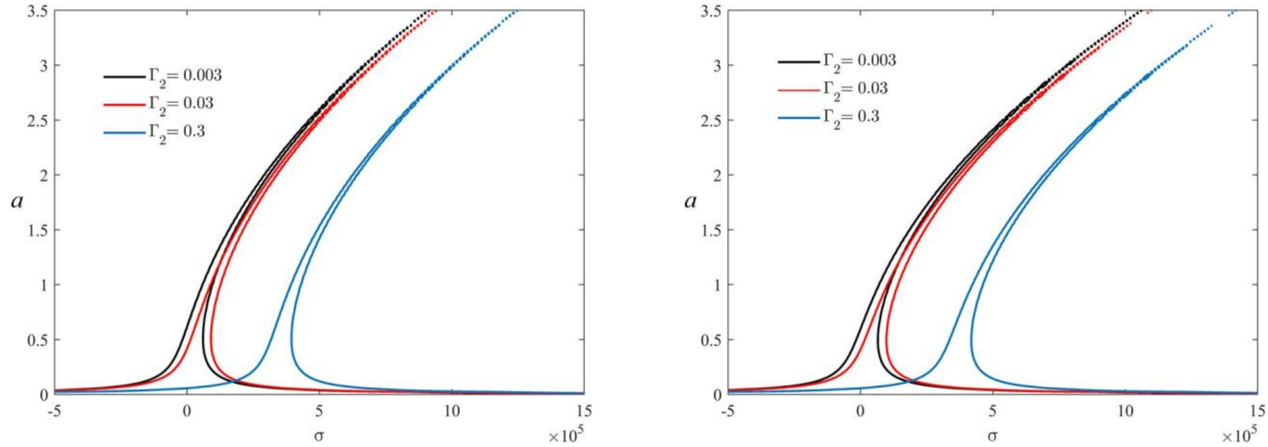

(a) External stiffeners (b) Internal stiffeners

Fig. 11 Effect of the excitation amplitudes on the frequency response curves of the SSFG cylindrical shell ($K = K_s = 1, \theta = 0°, \beta = 90°$)

- The hardening nonlinearity behavior of the system is most than other cases when angles of the stiffener are between 0° and 30°, whereas the hardening nonlinearity behavior is less than other cases when the stiffener angles are between 60° and 90°.
- The nonlinearity behavior of the system with external and internal stiffeners is respectively increased and decreased when the volume fraction index is increased.
- The ceramic cylindrical shells with the metal stiffeners have more hardening nonlinearity behavior than the others, and the metallic cylindrical shells with the ceramic stiffeners have less hardening nonlinearity behavior than the others.
- The hardening nonlinearity behavior of SSFG system increases by increasing the imperfection amplitude parameter.
- The hardening nonlinearity behavior of the system with the Pasternak foundation is larger than the hardening nonlinearity behavior of the system with the Winkler's foundation.
- The negative and positive nonlinear elastic foundation decreases and increases the hardening nonlinearity behavior of the system, respectively.
- The hardening nonlinearity behavior of system with the linear elastic foundation is decreased more than the system with nonlinear elastic foundation.
- Increasing the amplitude excitation Γ_1 leads to scaling up the frequency-response curve.
- By increasing the amplitude excitation Γ_2, the jumping phenomenon is transferred to higher values of σ.

References

Abe, A., Kobayashi, Y. and Yamada, G. (2007), "Nonlinear dynamic behaviors of clamped laminated shallow shells with one-to-one internal resonance", *J. Sound Vib.*, **304**, 957-968. https://doi.org/10.1016/j.jsv.2007.03.009.

Ahmadi, H. (2018), "Nonlinear primary resonance of imperfect spiral stiffened functionally graded cylindrical shells surrounded by damping and nonlinear elastic foundation", *Eng. Comput.*, 1-15. https://doi.org/10.1007/s00366-018-0679-2.

Ahmadi, H. and Foroutan, K. (2019a), "Nonlinear primary resonance of spiral stiffened functionally graded cylindrical shells with damping force using the method of multiple scales", *Thin Wall. Struct.*, **135**, 33-44. https://doi.org/10.1016/j.tws.2018.10.028.

Ahmadi, H. and Foroutan, K. (2019b), "Superharmonic and subharmonic resonances of spiral stiffened functionally graded cylindrical shells under harmonic excitation", *J. Struct. Stability Dynamics*. https://doi.org/10.1142/S0219455419501141.

Ahmadi, H. and Foroutan, K. (2019c), "Combination resonance analysis of FG porous cylindrical shell under two-term excitation", *Steel Compos. Struct*., **32**(2), 253-264. https://doi.org/10.12989/scs.2019.32.2.253.

Alijani, F., Amabili, M. and Bakhtiari-Nejad, F. (2011), "On the accuracy of the multiple scales method for non-linear vibrations of doubly curved shallow shells", *Int. J. Nonlin. Mech.*, **46**, 170-179. https://doi.org/10.1016/j.ijnonlinmec.2010.08.006.

Bich, D.H., Van Dung, D., Nam, V.H. and Phuong, N.T. (2013), "Nonlinear static and dynamic buckling analysis of imperfect eccentrically stiffened functionally graded circular cylindrical thin shells under axial compression", *Int. J. Mech. Sci.*, **74**, 190-200. https://doi.org/10.1016/j.ijmecsci.2013.06.002.

Dai, H.L., Dai, T. and Zheng, H.Y. (2013), "Creep buckling and post-buckling analyses for a hybrid laminated viscoelastic FGM cylindrical shell under in-plane loading", *Int. J. Mech. Mater. Des.*, **9**(4), 309-323. https://doi.org/10.1007/s10999-013-9223-0.

Dat, N.D., Quan, T.Q. and Duc, N.D. (2019), "Nonlinear thermal vibration of carbon nanotube polymer composite elliptical cylindrical shells", *Int. J. Mech. Mater. Des.*, 1-20. https://doi.org/10.1007/s10999-019-09464-y.

Du, C. and Li, Y. (2013), "Nonlinear resonance behavior of functionally graded cylindrical shells in thermal environments", *Compos. Struct.*, **102**, 164-174. https://doi.org/10.1016/j.compstruct.2013.02.028.

Eslami, M.R. (2018), *Buckling and Postbuckling of Beams, Plates, and Shells*, Springer International Publishing, Switzerland.

Eslami, M.R., Shariyat, M. and Shakeri, M. (1998), "Layerwise theory for dynamic buckling and postbuckling of laminated composite cylindrical shells", *AIAA J.*, **36**, 1874-1882. https://doi.org/10.2514/2.281.

Foroutan, K., Shaterzadeh, A. and Ahmadi, H. (2018), "Nonlinear dynamic analysis of spiral stiffened functionally graded cylindrical shells with damping and nonlinear elastic foundation under axial compression", *Struct. Eng. Mech.*, **66**(3), 295-303. https://doi.org/10.12989/sem.2018.66.3.295.

Gao, K., Huang, Q., Kitipornchai, S. and Yang, J. (2019), "Nonlinear dynamic buckling of functionally graded porous beams", *Mech. Adv. Mat. Struct.*, 1-12. https://doi.org/10.1080/15376494.2019.1567888.

Gao, K., Gao, W., Chen, D. and Yang, J. (2018a), "Nonlinear free vibration of functionally graded graphene platelets reinforced porous nanocomposite plates resting on elastic foundation", *Compos. Struct.*, **204**, 831-846. https://doi.org/10.1016/j.compstruct.2018.08.013.

Gao, K., Gao, W., Wu, B., Wu, D. and Song, C. (2018), "Nonlinear primary resonance of functionally graded porous cylindrical shells using the method of multiple scales", *Thin Wall. Struct.*, **125**, 281-293. https://doi.org/10.1016/j.tws.2017.12.039.

Gao, K., Gao, W., Wu, D. and Song, C. (2017), "Nonlinear dynamic characteristics and stability of composite orthotropic plate on elastic foundation under thermal environment", *Compos. Struct.*, **168**, 619-632. https://doi.org/10.1016/j.compstruct.2017.02.054.

Gao, K., Gao, W., Wu, D. and Song, C. (2018b), "Nonlinear dynamic stability of the orthotropic functionally graded cylindrical shell surrounded by Winkler-Pasternak elastic foundation subjected to a linearly increasing load", *J. Sound Vib.*, **415**, 147-168. https://doi.org/10.1016/j.jsv.2017.11.038.

Gao, K., Li, R. and Yang, J. (2019), "Dynamic characteristics of functionally graded porous beams with interval material properties", *Eng. Struct.*, **197**, 109441. https://doi.org/10.1016/j.engstruct.2019.109441.

Huang, B.W., Yu, P.P. and Jou, J.M. (2008), "Parametric resonance of a rotating taper pre-twisted beam with cracks", *Struct. Eng. Mech.*, **28**(2), 259-262. https://doi.org/10.12989/sem.2008.28.2.259.

Kumar, R., Kumar, A. and Panda, S.K. (2015), "Parametric resonance of composite skew plate under non-uniform in-plane loading", *Struct. Eng. Mech.*, **55**(2), 435-459. https://doi.org/10.12989/sem.2015.55.2.435.

Lezgy-Nazargah, M., Shariyat, M. and Beheshti-Aval, S.B. (2011), "A refined high-order global-local theory for finite element bending and vibration analyses of the laminated composite beams", *Acta Mech.*, **217**(3-4), 219-242. https://doi.org/10.1007/s00419-012-0621-9.

Li, F.M. and Yao, G. (2013), "1/3 Subharmonic resonance of a nonlinear composite laminated cylindrical shell in subsonic air flow", *Compos. Struct.*, **100**, 249-256. https://doi.org/10.1016/j.compstruct.2012.12.035.

Li, X., Du, C.C. and Li, Y.H. (2018), "Parametric resonance of a FG cylindrical thin shell with periodic rotating angular speeds in

thermal environment", *Appl. Math. Model.*, **59**, 393-409. https://doi.org/10.1016/j.apm.2018.01.048.
Mahmoudkhani, S., Navazi, H.M. and Haddadpour, H. (2011), "An analytical study of the non-linear vibrations of cylindrical shells", *J. Nonlin. Mech.*, **46**, 1361-1372. https://doi.org/10.1016/j.ijnonlinmec.2011.07.012.
Mustafa, B.A.J. and Ali, R. (1989), "An energy method for free vibration analysis of stiffened circular cylindrical shells", *Comput. Struct.*, **32**, 355-363. https://doi.org/10.1016/0045-7949(89)90047-3.
Nayfeh, A.H. and Mook D.T. (1995), *Nonlinear Oscilations*, John Wiley and Sons, New Jersey, USA.
Pendhari, S.S., Kant, T., Desai, Y.M. and Subbaiah, C.V. (2012), "Static solutions for functionally graded simply supported plates", *J. Mech. Mater. Des.*, **8**(1), 51-69. https://doi.org/10.1007/s10999-011-9175-1.
Pellicano F. (2007), "Vibrations of circular cylindrical shells: theory and experiments", *J. Sound Vib.*, **303**(1-2), 154-170. https://doi.org/10.1016/j.jsv.2007.01.022.
Qin, Z. Chu, F. and Zu, J. (2017), "Free vibrations of cylindrical shells with arbitrary boundary conditions: A comparison study", *Int. J. Mech. Sci.*, **133** 91-99. https://doi.org/10.1016/j.ijmecsci.2017.08.012.
Rodrigues, L., Gonçalves, P.B. and Silva, F.M.A. (2017), "Internal resonances in a transversally excited imperfect circular cylindrical shell", *Pro. Eng.*, **199**, 838-843. https://doi.org/10.1016/j.proeng.2017.09.010.
Sarigul, M. and Boyaci, H. (2010), "Nonlinear vibrations of axially moving beams with multiple concentrated masses Part I: primary resonance", *Struct. Eng. Mech.*, **36**(2), 149-163. https://doi.org/10.12989/sem.2010.36.2.149.
Shariyat, M. (2011), "Non-linear dynamic thermo-mechanical buckling analysis of the imperfect laminated and sandwich cylindrical shells based on a global-local theory inherently suitable for non-linear analyses", *Int. J. Non-Lin. Mech.*, **46**, 253-271. https://doi.org/10.1016/j.ijnonlinmec.2010.09.006.
Shaterzadeh, A. and Foroutan, K. (2016), "Post-buckling of cylindrical shells with spiral stiffeners under elastic foundation", *Struct. Eng. Mech.*, **60**, 615-631. https://doi.org/10.12989/sem.2016.60.4.615.
Shen, H.S. (2017), *Postbuckling Behavior of Plates and Shells*, World Scientific, Singapore.
Sheng, G.G. and Wang, X. (2018a), "Nonlinear vibrations of FG cylindrical shells subjected to parametric and external excitations", *Compos. Struct.*, **191**, 78-88. https://doi.org/10.1016/j.compstruct.2018.02.018.
Sheng, G.G. and Wang, X. (2018b), "The dynamic stability and nonlinear vibration analysis of stiffened functionally graded cylindrical shells", *Appl. Math. Model.*, **56**, 389-403. https://doi.org/10.1016/j.apm.2017.12.021.
Sofiyev, A.H. (2016), "Large amplitude vibration of FGM orthotropic cylindrical shells interacting with the nonlinear Winkler elastic foundation", *Compos. Part B*, **98**, 141-50. https://doi.org/10.1016/j.compositesb.2016.05.018.
Sofiyev, A.H., Avcar, M., Ozyigit, P. and Adigozel, S. (2009), "The Free Vibration of non-homogeneous truncated conical shells on a winkler foundation", *Int. J. Eng. Appl. Sci.*, **1**, 34-41.
Sofiyev, A.H., Hui, D., Haciyev, V.C., Erdem, H., Yuan, G.Q., Schnack, E. and Guldal, V. (2017), "The nonlinear vibration of orthotropic functionally graded cylindrical shells surrounded by an elastic foundation within first order shear deformation theory", *Compos. Part B*, **116**, 170-85. https://doi.org/10.1016/j.compositesb.2017.02.006.
Udar, R.S. and Datta, P.K. (2007), "Dynamic combination resonance characteristics of doubly curved panels subjected to non-uniform tensile edge loading with damping", *Struct. Eng. Mech.*, **25**(4), 481-500. https://doi.org/10.12989/sem.2007.25.4.481.
Van Dung, D. and Hoa, L.K. (2013), "Nonlinear buckling and post-buckling analysis of eccentrically stiffened functionally graded circular cylindrical shells under external pressure", *Thin Wall. Struct.*, **63**,117-124. https://doi.org/10.1016/j.tws.2012.09.010.
Van Dung, D. and Nam, V.H. (2014), "Nonlinear dynamic analysis of eccentrically stiffened functionally graded circular cylindrical thin shells under external pressure and surrounded by an elastic medium", *Eur. J. Mech. A-Solid*, **46**, 42-53. https://doi.org/10.1016/j.euromechsol.2014.02.008.
Wang, Y.Q., Liang, L. and Guo, X.H. (2013), "Internal resonance of axially moving laminated circular cylindrical shells", *J. Sound Vib.*, **332**, 6434-6450. https://doi.org/10.1016/j.jsv.2013.07.007.
Wang, Y.Q., Ye, Ch. and Zu, J.W. (2019), "Vibration analysis of circular cylindrical shells made of metal foams under various boundary conditions", *Int. J. Mech. Mater. Des.*, **15**(2), 333-344. https://doi.org/10.1007/s10999-018-9415-8.
Zhang, W., Liu, T., Xi, A. and Wang, Y.N. (2018), "Resonant responses and chaotic dynamics of composite laminated circular cylindrical shell with membranes", *J. Sound Vib.*, **423**, 65-99. https://doi.org/10.1016/j.jsv.2018.02.049.
Zarouni, E., Rad, M.J. and Tohidi, H. (2014), "Free vibration analysis of fiber reinforced composite conical shells resting on Pasternak-type elastic foundation using Ritz and Galerkin methods", *Int. J. Mech. Mater. Des.*, **10**(4), 421-438. https://doi.org/10.1007/s10999-014-9254-1.

PL

Appendix A

The H matrix of Eq. (7) is:

$$
\begin{aligned}
H_{11} &= \cos^3\theta + \cos^3\beta \\
H_{21} &= \sin\theta\cos^2\theta + \sin\beta\cos^2\beta \\
H_{31} &= \cos^2\theta - \cos^2\beta \\
H_{12} &= \sin^2\theta\cos\theta + \sin^2\beta\cos\beta \\
H_{22} &= \sin^3\theta + \sin^3\beta \\
H_{32} &= \sin\theta\cos\theta + \sin\beta\cos\beta \\
H_{13} &= 2\ \sin\theta\cos^2\theta - \sin\beta\cos^2\beta \\
H_{23} &= 2\ \sin^2\theta\cos\theta - \sin^2\beta\cos\beta \\
H_{33} &= \sin^2\theta - \sin^2\beta
\end{aligned}
\tag{A.1}
$$

where

$$
\begin{Bmatrix} h_1 \\ h_2 \\ h_3 \end{Bmatrix} = \frac{h_s dE_s}{sh_s}\sin\ \theta+\beta \begin{Bmatrix} 1/\ \sin\theta+\sin\beta \\ 1/\ \cos\theta+\cos\beta \\ 1/2 \end{Bmatrix}
\tag{A.2}
$$

Appendix B

The new parameters of Eqs. (11) and (12) may be defined as (Foroutan *et al.* 2018, Shaterzadeh and Foroutan 2016)

$$
\begin{aligned}
A &= J_{11}^{*}m^4\pi^4 + \ J_{33}^{*} - J_{12}^{*} - J_{21}^{*}\ \ m^2n^2\pi^2\lambda^2 + J_{22}^{*}n^4\lambda^4 \\
B &= J_{21}^{**}m^4\pi^4 + \ J_{11}^{*} + J_{22}^{*} - 2J_{36}^{**}\ \ m^2n^2\pi^2\lambda^2 \\
&\quad + J_{12}^{**}n^4\lambda^4 - \frac{L^2}{R}m^2n^2 \\
B^{*} &= A_{21}^{*}m^4\pi^4 + \ A_{11}^{*} + A_{22}^{*} - 2J_{36}^{**}\ \ m^2n^2\pi^2\lambda^2 \\
&\quad + J_{12}^{**}n^4\lambda^4 - \frac{L^2}{R}m^2n^2 \\
D &= A_{11}^{**}m^4\pi^4 + \ A_{12}^{**} + A_{21}^{**} + 4A_{36}^{**}\ \ m^2n^2\pi^2\lambda^2 \\
&\quad + A_{22}^{**}n^4\lambda^4 \\
G &= \left(\frac{n^4\lambda^4}{16J_{11}^{*}} + \frac{m^4\pi^4}{16J_{22}^{*}}\right),\ \lambda = \frac{L}{R}
\end{aligned}
\tag{B.1}
$$

where

$$
\begin{aligned}
&\Delta = J_{11}J_{22} - J_{12}J_{21} \quad J_{22}^{*} = \frac{J_{22}}{\Delta} \quad J_{12}^{*} = \frac{J_{12}}{\Delta} \\
&J_{11}^{*} = \frac{J_{11}}{\Delta} \quad J_{21}^{*} = \frac{J_{21}}{\Delta} \quad J_{33}^{*} = \frac{1}{J_{33}} \quad J_{36}^{*} = \frac{J_{36}}{J_{33}} \\
&J_{11}^{**} = J_{22}^{*}J_{14} - J_{12}^{*}J_{24} \quad J_{12}^{**} = J_{22}^{*}J_{15} - J_{12}^{*}J_{25} \\
&J_{21}^{**} = J_{11}^{*}J_{24} - J_{21}^{*}J_{14} \quad J_{22}^{**} = J_{11}^{*}J_{25} - J_{21}^{*}J_{15} \\
&A_{11}^{*} = J_{22}^{*}J_{14} - J_{21}^{*}J_{15} \quad A_{21}^{*} = J_{11}^{*}J_{15} - J_{12}^{*}J_{14} \\
&A_{12}^{*} = J_{22}^{*}J_{24} - J_{21}^{*}J_{25} \quad A_{22}^{*} = J_{11}^{*}J_{25} - J_{12}^{*}J_{24} \\
&A_{11}^{**} = J_{11}^{**}J_{14} - J_{21}^{**}J_{15} - J_{41} \\
&A_{12}^{**} = J_{12}^{**}J_{14} - J_{22}^{**}J_{15} - J_{42} \\
&A_{21}^{**} = J_{11}^{**}J_{24} - J_{21}^{**}J_{25} - J_{51} \\
&A_{22}^{**} = J_{12}^{**}J_{24} - J_{22}^{**}J_{25} - J_{52} \\
&A_{36}^{**} = J_{36}^{**}J_{36} - J_{63}
\end{aligned}
\tag{B.2}
$$

and

$$
\begin{aligned}
J_{12} &= \frac{E_1\nu}{1-\nu^2} + Z_1E_{1s}\left(\sin^2\theta\cos\theta + \sin^2\beta\cos\beta\right) \\
J_{15} &= \frac{E_2\nu}{1-\nu^2} + Z_1E_{2s}\left(\sin^2\theta\cos\theta + \sin^2\beta\cos\beta\right) \\
J_{21} &= \frac{E_1\nu}{1-\nu^2} + Z_2E_{1s}\left(\sin\theta\cos^2\theta + \sin\beta\cos^2\beta\right) \\
J_{24} &= \frac{E_2\nu}{1-\nu^2} + Z_2E_{2s}\left(\sin\theta\cos^2\theta + \sin\beta\cos^2\beta\right) \\
J_{33} &= \frac{E_1}{2(1+\nu)} + 2Z_3E_{1s}\left(\sin\theta\cos\theta + \sin\beta\cos\beta\right) \\
J_{36} &= \frac{E_2}{2(1+\nu)} + 2Z_3E_{2s}\left(\sin\theta\cos\theta + \sin\beta\cos\beta\right) \\
J_{42} &= \frac{E_3\nu}{1-\nu^2} + Z_1E_{3s}\left(\sin^2\theta\cos\theta + \sin^2\beta\cos\beta\right) \\
J_{51} &= \frac{E_3\nu}{1-\nu^2} + Z_2E_{3s}\left(\sin\theta\cos^2\theta + \sin\beta\cos^2\beta\right) \\
J_{63} &= \frac{E_3}{2(1+\nu)} + 2Z_3E_{3s}\left(\sin\theta\cos\theta + \sin\beta\cos\beta\right) \\
J_{11} &= \frac{E_1}{1-\nu^2} + Z_1E_{1s}\left(\cos^3\theta + \cos^3\beta\right)? \\
J_{14} &= \frac{E_2}{1-\nu^2} + Z_1E_{2s}\left(\cos^3\theta + \cos^3\beta\right)? \\
J_{22} &= \frac{E_1}{1-\nu^2} + Z_2E_{1s}\left(\sin^3\theta + \sin^3\beta\right) \\
J_{25} &= \frac{E_2}{1-\nu^2} + Z_2E_{2s}\left(\sin^3\theta + \sin^3\beta\right) \\
J_{41} &= \frac{E_3}{1-\nu^2} + Z_1E_{3s}\left(\cos^3\theta + \cos^3\beta\right) \\
J_{55} &= \frac{E_3}{1-\nu^2} + Z_2E_{3s}\left(\sin^3\theta + \sin^3\beta\right)
\end{aligned}
\tag{B.3}
$$

where

$$
\begin{aligned}
Z_1 &= \frac{d\sin\ \theta+\beta}{s[\sin\ \theta\ +\sin\ \beta\ ]} \\
Z_2 &= \frac{d\sin\ \theta+\beta}{s[\mathrm{os}\ \theta\ +\cos\ \beta\ ]} \\
Z_3 &= \frac{d\sin\ \theta+\beta}{2s}
\end{aligned}
\tag{B.4}
$$

In Eq. (B.3):

$$
E_1 = \int_{-h/2}^{h/2} E_{sh}(z)dz = \left(E_c + \frac{E_m - E_c}{K_{sh}+1}\right)h
\tag{B.5}
$$

$$E_2 = \int_{-h/2}^{h/2} zE_{sh}(z)dz = \frac{(E_m - E_c)kh^2}{2(K_{sh}+1)(K_{sh}+2)}$$

$$E_3 = \int_{-\frac{h}{2}}^{\frac{h}{2}} z^2 E_{sh}(z)dz = \left[\frac{E_c}{12}\right.$$

$$\left.+(E_m - E_c)\left(\frac{1}{K_{sh}+3} + \frac{1}{K_{sh}+2} + \frac{1}{4K_{sh}+4}\right)\right] h^3$$

External Stiffeners:

$$E_{1s} = \int_{-\left(\frac{h}{2}+h_s\right)}^{-\frac{h}{2}} E_s(z)dz = \left(E_m + \frac{E_c - E_m}{K_{st}+1}\right) h_s$$

$$E_{2s} = \int_{-\left(\frac{h}{2}+h_s\right)}^{-\frac{h}{2}} zE_s(z)dz = \frac{E_m}{2}\ hh_s\left(\frac{h_s}{h}+1\right)$$

$$+(E_c - E_m)\ hh_s\left(\frac{1}{K_{st}+2}\frac{h_s}{h} + \frac{1}{2K_{st}+2}\right)$$

$$E_{3s} = \int_{-\left(\frac{h}{2}+h_s\right)}^{-\frac{h}{2}} z^2 E_s(z)dz =$$

$$\frac{E_m}{3} h_s^3\left(\frac{3}{4}\frac{h^2}{h_s^2} + \frac{3}{2}\frac{h}{h_s} + 1\right)$$

$$+(E_c - E_m)h_s^3\left[\frac{1}{K_{st}+3} + \frac{1}{K_{st}+2}\frac{h}{h_s}\right.$$

$$\left.+\frac{1}{4(K_{st}+1)}\frac{h^2}{h_s^2}\right]$$

Internal Stiffeners:

$$E_{1s} = \int_{\frac{h}{2}}^{\frac{h}{2}+h_s} E_s(z)dz = \left(E_c + \frac{E_m - E_c}{K_{st}+1}\right) h_s$$

$$E_{2s} = \int_{\frac{h}{2}}^{\frac{h}{2}+h_s} zE_s(z)dz = \frac{E_c}{2}\ hh_s\left(\frac{h_s}{h}+1\right)$$

$$+(E_m - E_c)\ hh_s\left(\frac{1}{K_{st}+2}\frac{h_s}{h} + \frac{1}{2K_{st}+2}\right)$$

$$E_{3s} = \int_{\frac{h}{2}}^{\frac{h}{2}+h_s} z^2 E_s(z)dz =$$

$$\frac{E_c}{3} h_s^3\left(\frac{3}{4}\frac{h^2}{h_s^2} + \frac{3}{2}\frac{h}{h_s} + 1\right)$$

$$+(E_m - E_c)h_s^3\left[\frac{1}{K_{st}+3} + \frac{1}{K_{st}+2}\frac{h}{h_s}\right.$$

$$\left.+\frac{1}{4(K_{st}+1)}\frac{h^2}{h_s^2}\right]$$